Proceedings of the ASME 2024 Pressure Vessels & Piping Conference PVP2024 July 29-August 2, 2024, Bellevue, Washington

# PVP2024-123473

# CASE STUDY ON A CRACKING FAILURE IN UNS N06693 WELD FOR STEAM GENERATOR APPLICATIONS

Tim Pickle<sup>1</sup>, Kok-Theng Kho<sup>2</sup>, Jorge Penso<sup>3</sup>, Zhenzhen Yu<sup>1</sup>

<sup>1</sup>Colorado School of Mines, Golden, CO, USA <sup>2</sup>Shell MDS Sdn Bhd, Malaysia <sup>3</sup>Shell Global Solutions (US) Inc., Houston, Texas, USA

#### **ABSTRACT**

UNS N06693 is a Ni-base alloy that provides metal dusting corrosion resistance in steam generator pipes with operating temperatures above 500°C. A crack failure occurred in a 6.5mm thick similar weld pipe joint, located at both fusion zone and heat affected zone, after about 10 years in service and 2 months after weld repair in adjacent weld, which warranted an investigation into possible root causes of failure. This study investigates the potential failure mechanisms that may arise during service (such as stress relaxation cracking, stress corrosion cracking, ductility dip cracking, and creep failure) for UNS N06693 in order to understand the observed cracking behavior. In this year, preliminary fractography, metallurgical characterization, thermodynamic and kinetic CALHAD simulations, and investigation into potential contributing factors (e.g., weld procedure specifications (WPS) and post weld heat treatment (PWHT)) to failure have been completed. The fracture surfaces indicate brittle, intergranular failure, such that no shear lips were observed, and radial lines (crack propagation) were primarily observed in weld fusion zone. Metallurgical characterization near the fracture surface is conducted to reveal the contributing factors to failure, such as intermetallic phases (e.g., Cr-rich α-phase) and distribution of carbide particles (e.g., intergranular chromium carbides), that may contribute to reduced cracking and sensitization resistance. Blocky, intergranular Cr-rich precipitates, either Cr-rich \alpha-phase or Crrich  $M_{23}C_{6.}$ , are observed behind secondary cracks. Based on the initial findings, contributing factors for failure considered are increase in tensile residual stresses due to nearby repair field weld and grain boundary embrittlement due to coarse, blocky Cr-rich phase that likely developed during initial PWHT and within the 10-year service window. In the following year, a more in-depth metallurgical characterization, discussion contributing causes and possible mitigation strategies for

improving microstructural stability and performance-based weldability (e.g., weld procedure and PWHT design), and conclusions with root cause analysis will be provided.

Keywords: Ni-base alloy, weld repair, metal dusting, stress corrosion cracking, stress relaxation cracking, creep failure

## 1. INTRODUCTION

Steam generator pipes in petrochemical industry demand materials with good resistance to high temperature corrosion (>500°C) and metal dusting resistance, such as UNS N06693 alloy compared to other UNS N06XXX alloys [1]. Metal dusting is an aggressive corrosion mechanism that consists of five main steps: 1) carbon transfer to surface and breakdown of oxide film protection, 2) direct carburization of alloy and carbon diffusion in alloy leading to stable carbide formation, 3) metastable carbide precipitation formation on internal carbide upon further carbon diffusion, 4) decomposition of metastable carbides into filamentous carbon and metal, and 5) formation of coke [2, 3]. Compared to other alloys in the same class of alloys, N06693 outperforms in metal dusting resistance at 650°C [4] and other corrosion tests[5] mostly due to higher Cr content and Al content that contributes to more effective passive layers, as specified in ASTM standard B166-19 [6]. However, in case of other types of corrosion, i.e. intergranular corrosion which can be tested according to the Huey test (65% boiling nitric acid medium for 48 hours), N06690 outperformed N06693 and N06600 [7].

Regarding in-service damage, stress corrosion cracking (SCC) (reported in N06600 and N06690 alloys [8-11]) and stress relaxation cracking (SRC) or strain aging cracking (SAC) in Ni-base alloys [12-14] are two potential mechanisms for failure since the cracking failure occurred within a couple months of service re-startup after a nearby repair weld (40 mm away) was completed 10 years after initial startup. The increase in tensile residual stress from repair welding could possibly

contribute to a stress-assisted failure mechanism in the cracked weld. The presence of corrosive media, elevated temperature. aging mechanisms, and tensile (both internal residual and external) stresses may contribute to either SCC, SRC/SAC, or both. Additionally, metal dusting may develop over time. With respect to SRC or SAC, the development of a susceptible microstructure is critical, namely the formation of precipitate free zones (PFZs) along grain boundaries [15]. Of interest to hot working, solution anneal and heat treatment temperatures, the precipitation of γ' occurs below a solvus temperature of 1000°C where partial recrystallization and strain localization may occur [16]. Studies on  $\gamma$ ' formation and aging as a function of temperature and time indicated the best temperatures to maximize aging is 800°C [17-19]. The γ' can coarsen rapidly at 950°C and dissolve above 1000°C [20]. The development of bimodal and trimodal distributions of γ' may influence hardening mechanisms and strain distribution depending on cooling rates from temperature above  $\gamma$ ' solvus [19]. A study on brittle cracking of N06693 alloy in a compressive stress state at 900°C indicated transgranular fracture, likely due to formation of  $\gamma$ ' precipitates that inhibit plasticity and contribute to brittle failure [20]. It was identified that cooling from solution anneal temperatures allowed for  $\gamma$ ' formation even at high quench rates. Additionally, Cr-rich α-particles were observed to form at 950°C due to supersaturation of Cr in  $\gamma$  austenite coinciding with nucleation of Al- and Ti-rich γ' [18, 21, 22]. Coarsening of Crrich particles can act as crack initiation sites and contributed to a decrease in ductility and strength after aging at 950°C [21]. For embrittling fracture to occur, precipitation of discrete Cr-rich αparticles on grain boundaries and other precipitates (e.g., M<sub>23</sub>C<sub>6</sub> and MX) may contribute to strain localization along PFZs. The cracking resistance in service is dependent on the microstructure (and oxide layers) that develops beforehand, influenced by weld procedure (e.g., cooling rates) and post weld heat treatment.

In this study, failure analysis is conducted on N06693 Nibase alloy tube weld (1/4", 6.5 mm thick) where fracture occurred after two months in service following repair (~10 years in service total) of a nearby weld with operating temperature of 550°C and internal process gas fluids CO and H<sub>2</sub>. The goal of is to identify root cause(s) for cracking mechanisms through metallurgical characterization, fractography and thermodynamic calculations. By revealing contributing factors to failure, mitigation solutions can be recommended.

## 2. MATERIALS AND METHODS

### 2.1 Material composition and failure samples

The UNS N06693 Ni-base alloy composition is shown in Table 1. The main alloying elements are Al, Nb, Cr and Fe. Prior to welding in the shop, the seamless tubes were delivered in an annealed condition. After completion of shop welding, the tubes were ground, post weld heat treated (PWHTed) and then shipped over to the plant. Prior to service implementation, the ground tube was field welded to a flat front semi-insulation plate in a transfer duct between a gasifier and syngas effluent cooler (SEC) on one side and then welded to another N06639 tube of the same dimensions. After roughly a 10-year service time, two inlet tubes

underwent weld repair 40 mm away from the ground weld that cracked (closer to process side). The repair welds were initiated to install more metal dusting resistant materials along the inlet tubes closer to the steam side near SEC. One of the two tubes cracked in ground weld within two months of repair welding.

TABLE 1: Chemical composition of N06693 alloy

Element	Wt%
Cr	27.0-31.0
Fe	2.5-6.0
Al	2.5-4.0
Nb	0.5-2.5
Mn	1.0 max
Ti	1.0 max
Cu	0.5 max.
Si	0.5 max
C	0.15 max
S	0.01 max

Figure 1 shows as-received half of the tube weld and other fractured samples cut from the pipe. The crack was in the ground weld centered 40 mm from the field weld with reinforcement, as seen in Figure 1 (a). The ground weld was completed in the shop prior to the initial field weld with reinforcement, likely to minimize flow disruptions and stress risers. A repair to the field weld was completed a few months prior to fracture of shop, ground weld. The first fracture surface analyzed is outlined by the red rectangle in Figure 1 (a) with crack terminating in the OD of the weld, and the second one outlined in blue in Figure 1 (b).

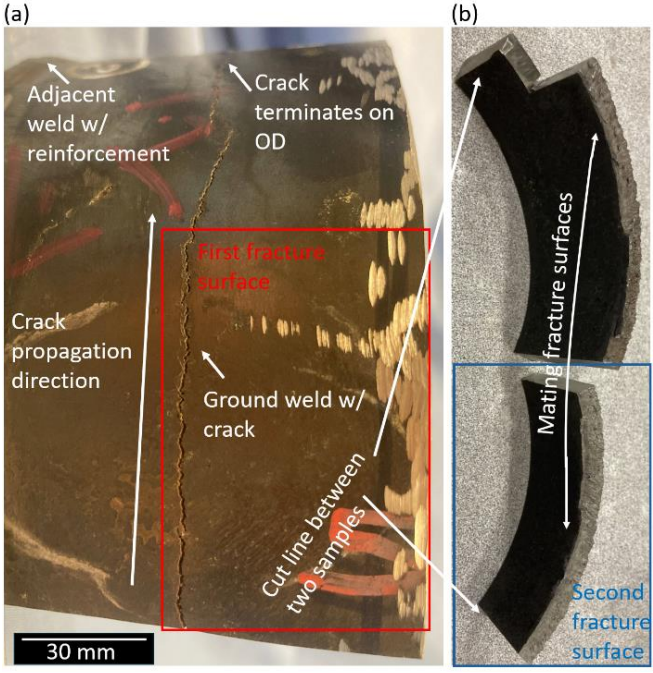


FIGURE 1: (a) Half-pipe section of cracked similar weld in N06693 pipe. The crack is located on a ground similar weld and crack terminated on OD. (b) Another cut section of fracture surfaces.

## 2.2 Welding and PWHT Procedures

The 6.5 mm seamless tubes were welded circumferentially according to the weld joint geometry in Figure 2. The weld joint is a single-V groove with a 60° groove angle and an open weld root gap of 2-3 mm. The process used for all welding passes was gas tungsten arc welding. The weld joint sequence was likely one root pass, a second layer of two passes, and a third capping layer with three passes. The amperage range is 100-180 amps with a 10-15 V range. It should be noted that the travel speed was specified in the procedure qualification record (PQR) as 0.66 mm/s, but the welding procedure specification (WPS) did not include a travel speed specification. The overall allowed heat input range, interchangeably used with arc energy, was 0.75-2.93 kJ/mm. The weld filler was matching filler (UNS N06693 with AWS A5.14 filler designation ERNiCrFeAl-1), and the weld was completed with argon shielding and backing gas.

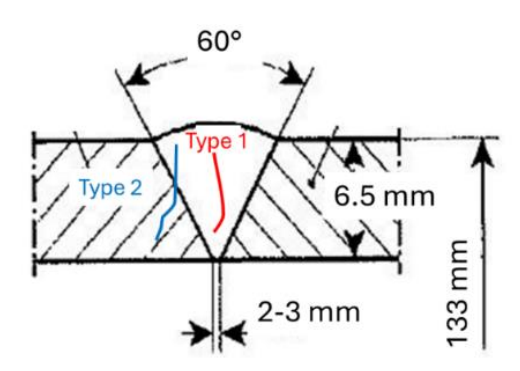


FIGURE 2: Weld joint geometry overlaid with crack types observed in cracking failure.

PWHT was conducted locally at the weld with 1040±10°C peak temperature for two hours using a heating rate of 120°C/h followed by air cooling. For clarity, this PWHT was completed in the shop. There is a discrepancy between WPS and PQR, where WPS states a 1040°C peak temperature but the POR states 950°C as the peak temperature. The intention of PWHT within 950-1050°C is to relieve stress and solutionize as-welded microstructure that later undergoes a service temperature of 538-760°C [1]. The PWHT procedure intentionally resets the microstructure, in addition to stress relief, prior to field welding of adjacent weld and further service conditions to avoid phases detrimental to low ductility and impact properties. After completion of welding and post processing of field welds, the weld underwent PD 5500 Cat 1 construction requirements, which includes non-destructive testing (NDT) using radiographic, dye penetrant, and visual testing techniques before and after PWHT. The NDT results reported in the WPS indicated no cracks, eliminating the concern for solidification or hot cracking.

# 2.3 Fractography and metallurgical characterization procedures

Fractography and metallurgical characterizations were performed using light optical microscopy (LOM) and scanning

electron microscopy secondary electron imaging (SEM-SEI) techniques. The fracture surfaces were examined on two samples with open cracks as seen in Figure 1 using preparation and preservation technique including ultrasonic cleaning in ethanol for five minutes and ultrasonic cleaning in 15g:350mL alconox to water ratio solution at 95°C for 30 minutes as described in [23]. Additionally, four cross section samples were analyzed as shown in Figure 3. LOM and SEM-EDS (electron dispersive spectroscopy) were used to identify crack paths and secondary phases. Microhardness, using Vicker's 500 g load, were conducted on samples 2 and 4 in the base metal, heat affected zone (HAZ), fusion zone (FZ) and weld regions in between.

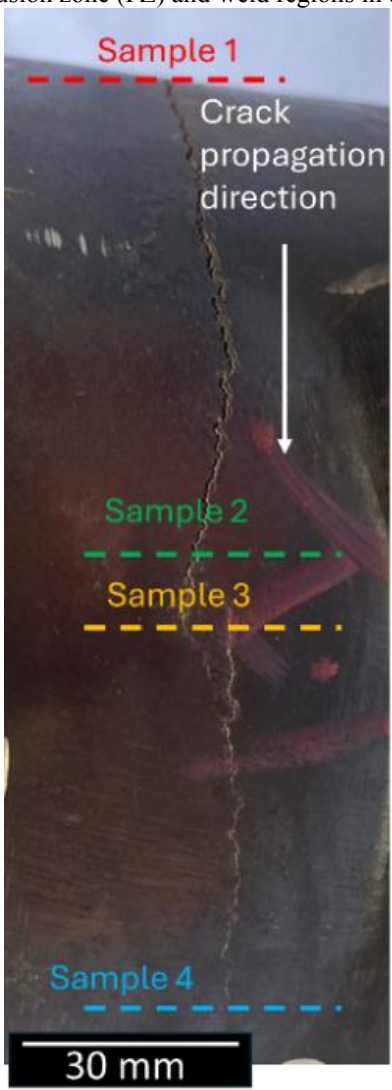


FIGURE 3: Optical micrograph showing four crosssectioning locations on pipe. Sample 4 is taken where crack propagation terminates.

## 2.4 CALPHAD calculations

Equilibrium and kinetic calculations are conducted using Thermo-Calc steels and Ni-alloys software package and TCFE13 and MOBFE7 databases. Equilibrium single axis diagrams and

time-temperature-transformation (TTT) curves were calculated at service- related temperature ranges from the equilibrium and precipitation calculators using PRISMA. X-ray fluorescence (XRF) measurement was performed on polished samples in midwall thickness to verify bulk composition in filler metal, and to provide the input composition for single-axis equilibrium and TTT curves. Carbon content was assumed to be 0.1 wt% for these calculations, since XRF cannot detect light elements.

# 3. RESULTS AND DISCUSSION

## 3.1 Fractography

Figure 4(a) shows the fractographic stitched image of two fracture surfaces along the same crack path, where the crack seems to initiate in the inner diameter (ID) of the pipe either in the weld FZ or HAZ. The crack propagates both radially outward towards the outer diameter (OD) and circumferentially. Some locations showed the cracks appearing to start in the fine grained HAZ and coarse grained HAZ on the ID and then transit into the FZ towards the OD. Generally, the fracture surfaces as shown in Figure 4 (b-c) are intergranular cracking in the HAZ and interdendritic cracking in the FZ. No microvoid coalescence was observed, and transgranular cleavage fracture was not evident on most of the fracture surfaces observed. Fracture surfaces were referenced with respect to fractographic examples shown in ASM Handbook Volume 11A [24]. However, the appearance of some slight marks on the ID may indicate crack initiation in the weld FZ as labeled by "possible initiation site" in Figure 4 (a).

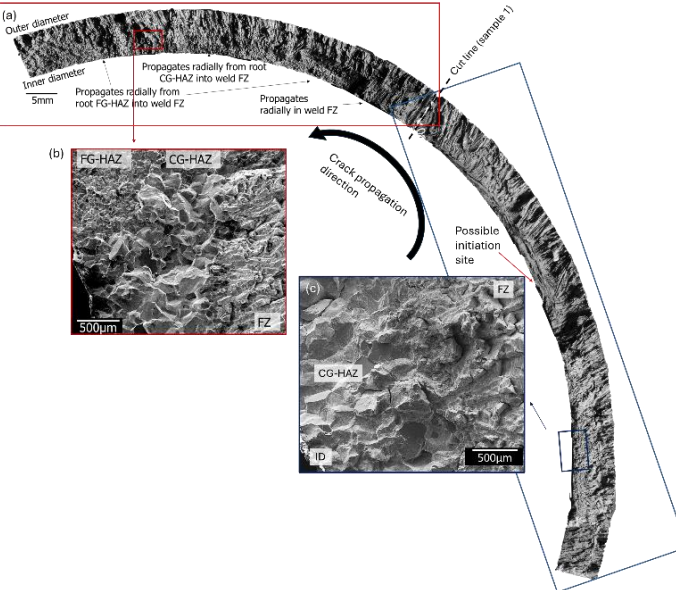
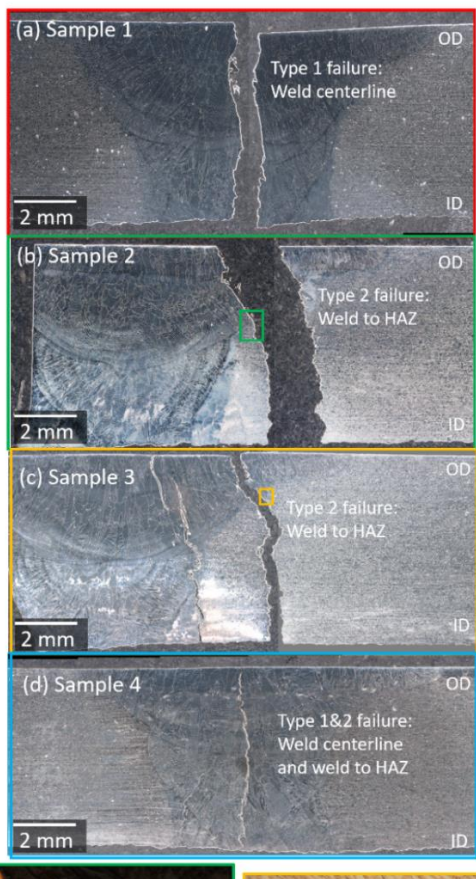


FIGURE 4: Fractography: (a) two macro fracture surfaces side by side, (b) SEM-SEI image showing intergranular fracture in HAZ of ID, (c) SEM-SEI image showing intergranular fracture on second sample

## 3.2 Metallurgical characterization

The etched macroscopic cross sections in Figure 5 (a-d) show the crack paths through thickness at various locations along the circumference. Sample 1 shows Type 1 failure along the weld

centerline, while sample 2 and 3 shows Type 2 failure either from the weld FZ to the HAZ or the opposite. Sample 4, where the crack terminates at the OD in the weld centerline, shows both Type 1 and 2 failure, with both centerline weld cracking and a crack going from HAZ on ID through the weld FZ, as seen in Figure 2. In all, fracture seems to initiate on the ID, propagate through thickness and terminate in the FZ in the OD. Figure 5 (e-f) shows some secondary intergranular and interdendritic cracking in the FZ and HAZ transition in samples 2 and 3.



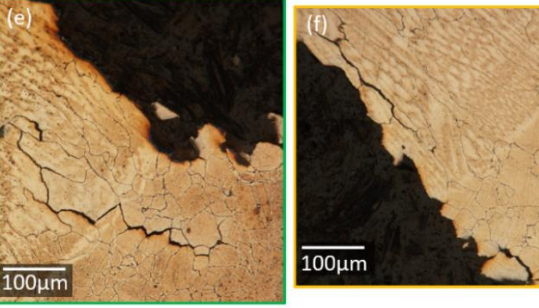


FIGURE 5: Optical micrographs of samples 1-4 cross sections (a-d) and secondary cracks in samples 2(e) and sample 3 (f).

Microhardness maps are overlayed on sample 2 and sample 4 in Figure 6 (a) and Figure (b), respectively. Two main observations can be made for both samples. The first observation is hardness increases from the OD to the ID in the base metal,

and the second observation is hardness increases in the coarse grained HAZ (CG-HAZ) and root pass FZ. Figure 6(c) shows the crack initiation locations on the ID in both the FZ and HAZ for sample 4, which correspond to the high hardness region. The microcrack initiation on ID seems to correlate with the high hardness regions in general. Higher microhardness regions are predictors of failure locations and likely indicate the possibility of more plastic deformation in the weld root regions, higher volume fraction of  $\gamma$  or carbonitrides, or both. Figure 6 (d) shows a higher magnification optical micrograph of the ID interface where crack initiates in CG-HAZ. The metal dusting layer can be observed to have a wavy, inconsistent thickness.

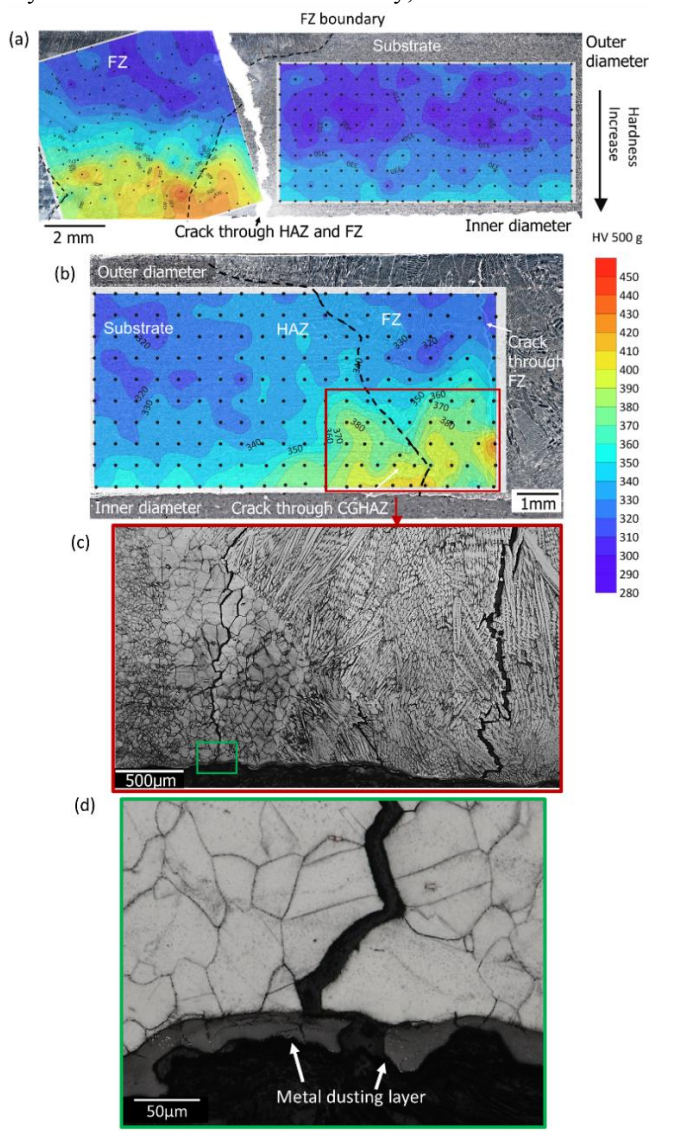


FIGURE 6: Microhardness maps of (a) sample 2 and (b) sample 4 weld cross sections, (c) optical micrographs of ID of sample 4 showing centerline FZ and CG-HAZ cracks initiating on the ID by oxalic electrolytic etch, and (d) higher magnification optical micrograph of CG-HAZ crack initiation on ID showing wavy metal dusting layer by Kroll's reagent etch.

Cr-rich precipitates are seen to be present mostly along grain boundaries in Figure 7 ahead of secondary cracks in CG-HAZ of sample 4. Blocky, discrete Cr-rich precipitates decorate the grain boundaries, as seen in Figure 7 (b). With respect to sensitization, Cr-depletion on grain boundaries may be present if Cr is tied up in a carbide (e.g.,  $M_{23}C_6$ ) or  $\alpha$  phase as a result of solutionizing, welding, and PWHT temperature and cooling rate conditions [21]. No obvious precipitate free zones (PFZs) were observed using the LOM and SEM methods.

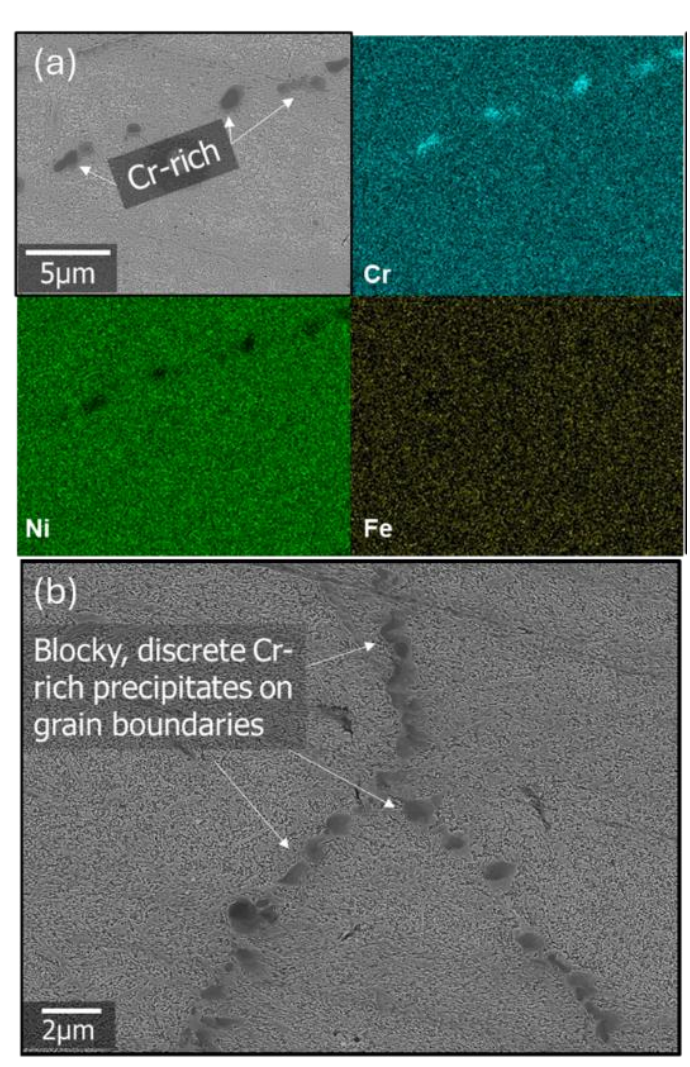


FIGURE 7: (a) Electron dispersive spectroscopy (EDS) map of sample 4 ahead of secondary crack tip in HAZ, and (b) triple point grain boundaries showing blocky Cr-carbides

The comparison between microstructures in the CG-HAZ and fine-grained-HAZ (FG-HAZ) is shown in Figure 8. Cr-rich precipitates are seen in both locations, and the size of  $\gamma$ ' is coarser in the CG-HAZ than that in the FG-HAZ. A bimodal distribution of  $\gamma$ ' seems to be present in both the CG-HAZ and FG-HAZ (as seen in Figure 8 (a, c)), which means there are both coarse and fine  $\gamma$ ' precipitates in both HAZ regions. Overall, the

γ' precipitate size appears coarser in the CG-HAZ. The aging of γ' primarily occurs during service conditions or during slow cooling from PWHT, since PWHT temperature (1040°C) is above the γ' solvus and does not include an aging step. The bimodal distribution can be attributed to coarse  $\gamma$ ' growth during cooling from welding or cooling from PWHT and fine  $\gamma$ ' particles may nucleate and grow during service temperatures. With respect to cracking mechanisms, the active aging of the microstructure without prior microstructural stability may influence cracking along grain boundaries via strain age cracking mechanism. In combination with active aging of intragranular  $\gamma'$ , the presence of blocky, intergranular Cr-rich precipitates may facilitate intergranular cracking via grain boundary sliding or creep void development along PFZs, which contributes to a strain aging cracking (SAC) or stress relaxation cracking (SRC) mechanism. On the other hand, Cr-rich intergranular precipitates could contribute to localized sensitization for SCC or embrittlement of grain boundaries.

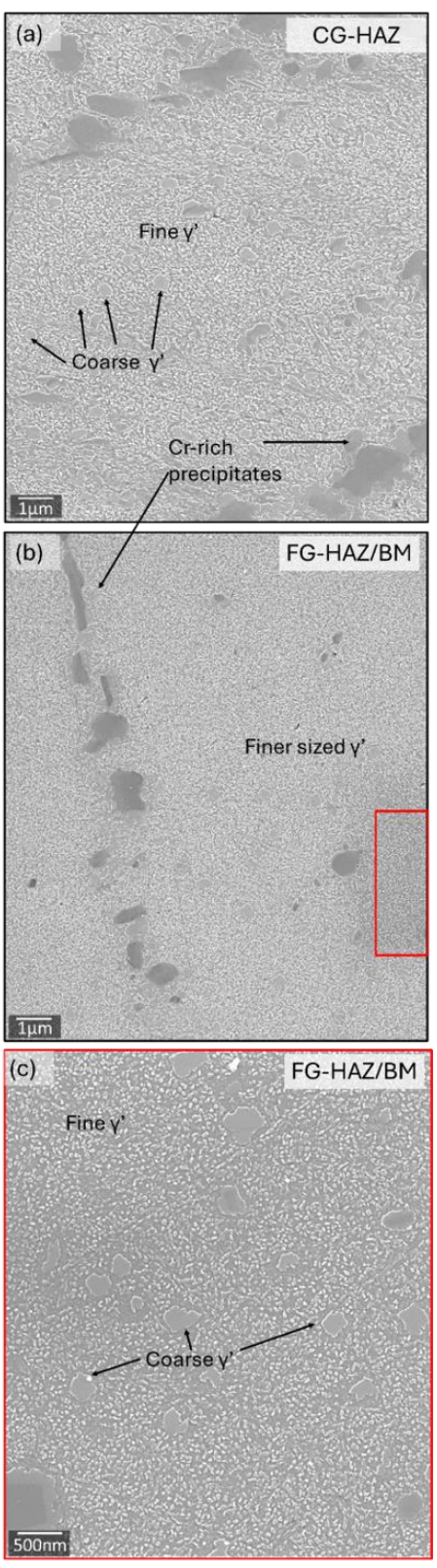


FIGURE 8: Higher mag SEM-SEI image of (a) CG-HAZ and (b) finer grained HAZ, with (c) higher mag image showing bimodal distribution of  $\gamma$  particles in sample 4.

### 3.3 CALPHAD simulations

The weld metal composition measured from XRF is summarized in Table 2 and compared to the base metal.

TABLE 2: Chemical compositions (in wt%) of base metal, weld filler measured using XRF. Compared to limit composition of UNS N06693 designation.

Element	Weld metal	Limit comp.
Cr	28.5	27.0-31.0
Fe	3.1	2.5-6.0
Al	2.9	2.5-4.0
Nb	0.6	0.5-2.5
Mn	0.2	1.0 max
Ti	0.3	1.0 max
Cu	0	0.5 max.
Si	0.3	0.5 max
С	NA	0.15 max
S	NA	0.01 max

CALPHAD equilibrium single axis diagram of weld metal, with a composition matching base metal standard limitations, is shown in Figure 9, based on XRF measurement and assumed carbon content of 0.1wt%. This assumption was based on the likelihood of potential carburization over a 10-year service period and a slight increase in microhardness from OD to ID in the base metal.  $\gamma'$  would be the second dominant phase to develop during elevated service temperatures or during slow cooling from PWHT. An equilibrium volume fraction of 0.35  $\gamma'$  is predicted to develop with a temperature of 550°C. Another phase that could develop during service conditions would be a Cr-rich BCC phase. Additionally, smaller volume fractions of  $M_{23}C_6$  and (Nb, Ti) C are predicted to develop, with  $M_{23}C_6$  having a wider temperature formation range of 500-1200°C and (Nb, Ti) C having a temperature range of 980-1310°C.

Figure 10 shows the TTT diagram for the weld filler region with overlayed PWHT and service temperature and time schedules. The matrix phase is γ-austenite and the stop criteria for the calculation is 0.5 of the equilibrium volume fraction of each phase, except for Cr-rich BCC, which has a much lower stop criteria of 0.0001 volume fraction. For instance, the equilibrium volume fraction of  $\gamma$ ' at 550°C is approximately 0.35, and the 50% equilibrium volume fraction stop criteria means the TTT calculation for γ' at 550°C is based on a 0.175 volume fraction. Peak nucleation and growth rates of M<sub>23</sub>C<sub>6</sub> and (Nb, Ti) C is predicted at a 1040°C PWHT temperature, while  $\gamma$ ' aging occurs mostly during service temperatures and during cooling from PWHT but not during isothermal hold since 1040°C is above the solvus for  $\gamma$ '. While the kinetics for Cr-rich BCC are very sluggish, the most likely phase to develop for a 10year period time period at service would be  $\gamma$ ' and M<sub>23</sub>C<sub>6</sub>. The failure time is indicated roughly by the "failed" symbol in Figure 10.

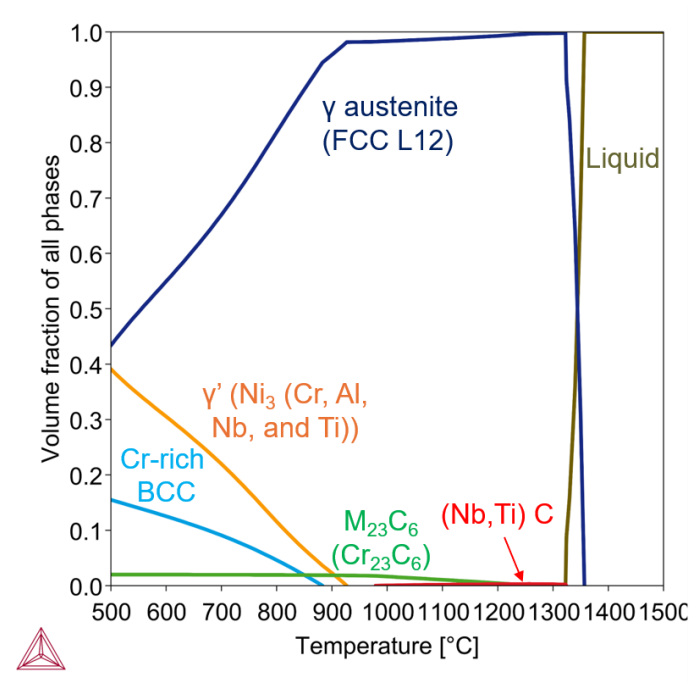


FIGURE 9: CALPHAD thermodynamic single axis equilibrium of weld filler composition showing volume fraction of phases as a function of temperature (assume C=0.1 wt%).

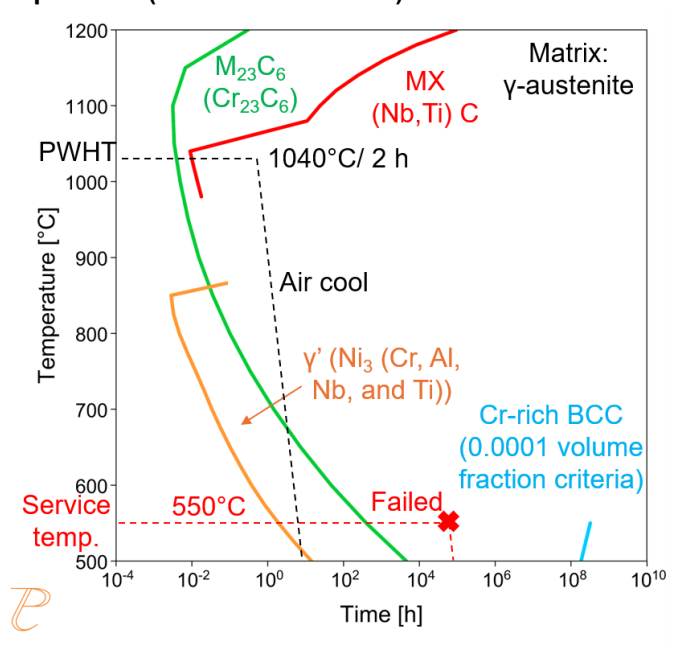


FIGURE 10: CALPHAD kinetic precipitation TTT diagram of weld filler composition (assume C=0.1 wt%). Stop criteria is equilibrium 50% volume fraction of each phase, except for Cr-rich BCC. PWHT and service temperatures are included for reference, and "failed" indicates the time the sample was in service prior to fracture.

# 3.3 Discussion on fracture mechanisms and possible mitigation solutions

The possible fracture mechanisms, based on the observations so far, could be mostly SRC (SAC) or SCC in addition to some evidence of mild corrosion on the ID (based on a wavier interface). The higher microhardness in the weld FZ may be attributed to a predictably higher  $\gamma$  volume fraction because of a slightly higher temperature on the ID (faster kinetics) versus the OD. Additionally, carburization of the ID during service, a possibility after a 10-year service, could potentially increase the strength and formation of fine M<sub>23</sub>C<sub>6</sub> precipitates that could increase strength. The concern for Crdepletion along grain boundaries with the formation of these carbides would contribute to sensitization and potentially SCC. 538°C was a prime temperature for intergranular carbide precipitation and possibly in SCC in alloy N06690, based on results using the Huey test (boiling nitric acid solution) [8]. The certainty of the mild corrosion behavior to cracking susceptibility is unknown, and there may be two different contributing mechanisms to failure. The observations of intergranular fracture do not eliminate SRC (SAC) and SCC as plausible contributing cracking mechanisms. The cooling rates and solutionizing temperatures in both processing of tubes and PWHT after welding influence the potential embrittling α Crrich phase in conjunction with nucleation and growth of  $\gamma$ ' during cooling from PWHT or time at service can influence cracking susceptibility or sensitization resistance during service. Cr-rich α phase can potentially reduce ductility and UTS of microstructure [21]. The next step of the analysis is to provide a more comprehensive assessment of the precipitation development and corrosion products in ID.

Modification of welding procedures and PWHT could possibly benefit the performance, even for joints influenced by local repair welding. First, the WPS for the shop weld allowed for higher than required heat input with a range of 0.75-2.93 kJ/mm, which exceeds the maximum heat input recommendation of 1.5 kJ/mm from ISO standard 15614-1[25]. Simply, the weld heat input needs to be maintained below 1.5 kJ/mm to minimize grain coarsening in the CG-HAZ, which can lead to a higher SRC susceptibility [13, 26] Additionally, too high of a PWHT temperature without stabilization of  $\gamma^{\circ}$  prior to service could contribute to SAC or SCC during service. Therefore, a potential recommended change to the PWHT would be to reduce the peak temperature to 1000°C followed by fast cooling to a second aging step at 750-800°C to stabilize microstructure prior to service conditions or subsequent manufacturing steps.

## 4. CONCLUSION

Failure analysis was conducted on N06693 ground weld steam generator pipes that failed after ten years of service and two months in service after repair welding in nearby field weld with operating temperature of 550°C. Fractography showed mostly intergranular cracking in the HAZ and interdendritic cracking in the FZ. Evidence points to crack initiation occurring on the ID in the root pass HAZ or FZ, which correlates with peak hardness regions. Crack propagation occurred through-thickness

along the pipe periphery and almost always terminate in the FZ on the OD. Blocky, discrete intergranular Cr-rich precipitates. which likely developed during 1040°C PWHT, may have increased cracking susceptibility in CG-HAZ with respect to SAC/SRC and SCC. Aging of γ', without prior aging steps in PWHT, during service temperatures in conjunction with embrittling Cr precipitates may possibly contribute to a SAC/SRC mechanism on grain boundaries. However, a PFZ has not been observed clearly in sample 4. A contributing cause to failure may be the repair weld generating an increase in tensile residual stresses in the nearby ground weld two months prior to fracture. An additional contributing cause to failure maybe an allowed high heat input during welding that could have contributed to sufficient grain growth, in which coarser grains are more detrimental for SRC. This increase in tensile residual stresses, combined with grain boundary embrittlement, contributed to an intergranular/interdendritic fracture. More analysis is planned to confirm whether SAC/SRC or SCC are the likely cracking mechanisms in addition to analysis on creep mechanisms and ductility dip cracking.

### 5. FUTURE PLAN

The future work necessary to provide a comprehensive failure analysis to determine root cause analysis:

- Precipitate analysis in weld regions for more in-depth characterization of secondary phases, including aging effect on γ', and determination of PFZs and creep voids.
- Analysis of oxide layer, metal dusting corrosion layer, corrosion products, and potential carburization on ID, in believed crack initiation location.

## **ACKNOWLEDGEMENTS**

This work is financially supported by the Manufacturing & Materials Joining Innovation Center (Ma<sup>2</sup>JIC), an industry and university cooperative research center (IUCRC) partially funded by the National Science Foundation (NSF) with award No, 2052819. Special thanks to Cameron Morey for assistance in metallography and fractography preparation and analysis.

### **REFERENCES**

- [1] INCONEL alloy 693-Excellent Resistance to Metal Dusting and High Temperatrue Corrosion. (2005).
- [2] H. J. Grabke, "Metal dusting," in *Corrosion by Carbon and Nitrogen: Metal Dusting, Carburisation and Nitridation*, M. M. The Institute of Materials Ed.: Woodhead and Maney Publishing, 2007, pp. 1-24.
- [3] C. M. Chun and T. A. Ramanarayanan, "The metal dusting corrosion of steels with varying concentrations of chromium," in *Corrosion by Carbon and Nitrogen: Metal Dusting, Carburisation and Nitridation*, M. M. The Institute of Materials Ed.: Woodhead and Maney Publishing, 2007, pp. 25-48.
- [4] C. M. Chun, G. Bhargava, and T. A. Ramanarayanan, "Metal Dusting Corrosion of Nickel-Based Alloys," *Journal of The Electrochemical Society*, vol. 154, no. 5, p. C231, 2007, doi: 10.1149/1.2710215.

- [5] S. A. McCoy, B. A. Baker, G. D. Smith, C. S. Tassen, P. Hazledine, and L. S. Shoemaker, "Nickel base alloys in high temperature applications in the petrochemical industry," in *Corrosion*, San Antonio, TX, 2014: NACE International.
- [6] *B166-19* A. International, 2019.
- [7] P. K. Samantaroy, "Intergranular Corrosion Behavior of Nickel Base Superalloys 600, 690, and 693," *International Journal of Engineering Research & Technology*, vol. 9, no. 1, pp. 470-474, 2020.
- [8] J. R. Crum, "Stress Corrosion Cracking Testing of Inconel Alloys 600 and 690 Under High Temperature Caustic Conditions," *Corrosion-NACE*, vol. 42, no. 6, pp. 368-372, 1986.
- [9] T. Moss, W. Kuang, and G. S. Was, "Stress corrosion crack initiation in Alloy 690 in high temperature water," *Current Opinion in Solid State and Materials Science*, vol. 22, no. 1, pp. 16-25, 2018, doi: 10.1016/j.cossms.2018.02.001.
- [10] K. Arioka, T. Yamada, T. Miyamato, and T. Terachi, "Dependence of Stress Corossion Cracking of Alloy 690 on Temperature, Cold Work, and Carbide Precipitation-Role of Difussion of Vacancies at Crack Tips," *Corrosion*, vol. 67, no. 3, 2011.
- [11] M. Casales, V. M. Salinas-Bravo, A. Martinez-Villafne, and J. G. Gonzalez-Rodriguez, "Effect of heat treatment on the stress corrosion cracking of Inconel 690," *Materials Science and Engineering: A*, vol. 332, pp. 223-230, 2002.
- [12] E. C. Dillingh, A. Bahrami, and A. P. Aulbers, "Stress Relaxation Cracking-Augmented Recommended Practice," TNO report, , 2016.
- [13] H. van Wortel, "Control of Relaxation Cracking in Austenitic High Temperature Components," presented at the NACE Corrosion, Nashville, TN, 2007.
- [14] J. A. Siefert, J. P. Shingledecker, J. N. DuPont, and S. A. David, "Weldability and weld performance of candidate nickel based superalloys for advanced ultrasupercritical fossil power plants Part II: weldability and cross-weld creep performance," (in English), *Science and Technology of Welding and Joining*, vol. 21, no. 5, pp. 397-428, 2016. [Online]. Available: <Go to ISI>://WOS:000376608600008.
- [15] R. Kant and J. N. DuPont, "Stress Relief Cracking Susceptibility in High-Temperature Alloys," *Welding Journal*, vol. 98, no. 2, pp. 29-49, 2019, doi: 10.29391/2019.98.003.
- [16] J. B. Singh, A. Verma, M. K. Thota, and R. Kapoor, "Dynamic recrystallization during hot-deformation of a

- newly developed Alloy 693," *Materials Characterization*, vol. 167, p. 110529, 2020, doi: 10.1016/j.matchar.2020.110529.
- [17] S. Khan, J. B. Singh, and A. Verma, "Age hardening behaviour of Alloy 693," *Materials Science and Engineering: A*, vol. 697, pp. 86-94, 2017, doi: 10.1016/j.msea.2017.04.109.
- [18] R. S. Dutta, A. Sarkar, B. Vishwanadh, R. Tewari, P. U. Sastry, and G. K. Dey, "Precipitation-hardening of superalloy 693 and modeling of initial stages of hardening," *Materials Characterization*, vol. 138, pp. 127-135, 2018, doi: 10.1016/j.matchar.2018.02.007.
- [19] S. Khan, J. B. Singh, and A. Verma, "Precipitation behaviour of γ' phase in Alloy 693," *Materials Characterization*, vol. 119, pp. 24-33, 2016, doi: 10.1016/j.matchar.2016.07.007.
- [20] J. B. Singh, A. Verma, M. K. Thota, and J. K. Chakravartty, "Brittle failure of Alloy 693 at elevated temperatures," *Materials Science and Engineering: A*, vol. 616, pp. 88-92, 2014, doi: 10.1016/j.msea.2014.08.015.
- [21] S. Khan, J. B. Singh, A. Verma, and M. Karri, "Precipitation of a chromium-rich α-phase in Alloy 693 and its effect on tensile properties," *Materials Science and Engineering: A*, vol. 686, pp. 176-183, 2017, doi: 10.1016/j.msea.2017.01.013.
- [22] P. K. Samantaroy, S. Girija, and U. K. Mudali, "Effect of Heat Treatment on Corrosion Behavior of Alloy 690 and Alloy 693 in Simualted Nuclear High-Level Waste Medium," *Corrosion*, vol. 48, no. 4, 2012.
- [23] R. D. Zipp and E. P. Dahlberg, "Preparation and Preservation of Fracture Specimens," in *ASM Handbook*, vol. 12: Fractography: ASM International, 1987, pp. 72-77.
- [24] L. A. Ganhao, J. J. Perdomo, J. McVay, and A. Seijas, "Failures of Pressure Vessels and Process Piping," in *ASM Handbook*, vol. 11A, Analysis and Prevention of Component and Equipment Failures: ASM International, 2021, pp. 565-637.
- [25] ISO 15614-1:Specification and qualification of welding procedures for metallic materials-Welding procedure test, ISO, Switzerland 2017.
- [26] L. S. Shoemaker, G. D. Smith, B. A. Baker, and J. M. Poole, "Fabricating Nickel Alloys to Avoid Stress Relaxation Cracking," in *Corrosion 2007*, Houston, TX, N. International, Ed., 2007, vol. 07421: NACE International.